Electronic Supplementary Information

Charge-Redistributed $Co_3O_4/Fe_{0.3}Co_{0.7}P$ Heterointerfaces for Efficient Electrocatalytic Urea Oxidation

Shan Zhang[a], Ming Zhao[a], Xiaoyan Zhang[b], Chao Wang[c], Chunmei Zhang[a], Huanhuan Xing[a], Chunzi Yang[a], Ruguang Ma[a*] and Chunxian Guo[a*]

[a] *Institute of Materials Science and Devices, School of Materials Science and Engineering, Suzhou University of Science and Technology, Suzhou 215011, China.*

[b] *College of Chemistry and Chemical Engineering, Qingdao University, Qingdao 266071, P. R. China.*

[c] The Russell H. Morgan Department of Radiology and Radiological Science, The Johns Hopkins University School of Medicine, Baltimore, Maryland 21218-2625, United States.

Experimental Section

Chemicals and Reagents

The nickel foam (NF) was purchased from Shenzhen Green and Creative Environmental Science and Technology Co., Ltd and utilized as substrate to grow various nanomaterials. Cobalt chloride hexahydrate ($CoCl_2 \cdot 6H_2O$) was bought from Aladdin (Shanghai, China). Urea and potassium ferricyanide ($K_3Fe(CN)_6$) were provided by Macklin (Shanghai, China). Sodium hypophosphite monohydrate ($NaH_2PO_2 \cdot H_2O$) was obtained from Sigma-Aldrich Chemical Reagent Co., Ltd. Other chemicals including HCl, KOH, ethanol and acetone were bought from Beijing Chemical Works. All chemicals and reagents were used as received unless noted, and the deionized water was purified through Millipore system.

Synthesis

Synthesis of CCHH: Firstly, the obtained NF was cut into small pieces of 2×3 cm^2, which underwent sonication successively in ethanol, acetone, 1 M HCl and water for 20 min, respectively, and then dried at 60°C overnight for further use. The synthetic procedure of CCHH was similar to that in our previous work. $CoCl_2 \cdot 6H_2O$ (0.285 g), urea (0.36 g) and 15 mL deionized water was completely mixed to form uniformly transparent solution. Thereafter, the solution was transferred into Teflon-lined autoclave with maximum capacity of 20 mL. Meanwhile, a piece of aforementioned NF was put into the autoclave. Then the autoclave was sealed and heated at 80°C for 12 h. After cooling down naturally, the obtained CCHH was washed in water by sonication for several minutes, then dried in oven at the temperature of 60°C.

Synthesis of CCHH/$FeCo_2(CN)_6$: $K_3Fe(CN)_6$ (0.12 g) was dissolved in 15 mL deionized water to obtain homogeneously yellow solution. Then it was transferred into 20 mL Teflon-lined autoclave with a piece of obtained CCHH. Afterward, the autoclave was sealed and heated to 60°C for 12 h and 18 h to prepare CCHH/$FeCo_2(CN)_6$ and $FeCo_2(CN)_6$, respectively. When cooling down to room temperature, they were collected and washed by sonication with water before dried at 60°C overnight.

Synthesis of $Co_3O_4/Fe_{0.3}Co_{0.7}P$: The obtained CCHH/$FeCo_2(CN)_6$ proceeded subsequent phosphating process to produce $Co_3O_4/Fe_{0.3}Co_{0.7}P$ heterostructure. Specifically, a piece of CCHH/$FeCo_2(CN)_6$ was put in the middle of the tube furnace with 1 g $NaH_2PO_2 \cdot H_2O$ placed at its upstream. Ar gas flowed through tube furnace for at least 30 mins to expel air completely. Then the tube furnace was heated to 350°C for 5 h at the heating rate of 5°C/min. Afterward, it cooled down to the room temperature under the protection of Ar to obtain $Co_3O_4/Fe_{0.3}Co_{0.7}P$. Similarly, $FeCo_2(CN)_6$ underwent the same phosphating process to prepare $Fe_{0.3}Co_{0.7}P$.

Synthesize of Co_3O_4: The pure Co_3O_4 was produced by calcining the pristine CCHH in the air at the temperature of 350°C for 2 h. The heating rate was slow down as 3°C/min to ensure fully calcination. The Co_3O_4 could be collected after cooling down to the room temperature naturally.

Characterization

Transmission electron microscopy (TEM) and high-resolution TEM (HRTEM) images were collected on JEM-2100F (Netherlands) at the voltage of 200 kV. Scanning electron microscopy (SEM) measurement was performed on PHILIPS XL-30 ESEM (20 kV). X-ray diffraction (XRD) profiles were obtained using Bruker D8A A25 (Cu Kα, λ = 1.5418 Å). X-ray photoelectron spectroscopy (XPS) was recorded on Thermo ESCALAB 250 instrument with Al Kα radiation.

Electrochemical measurements

All electrochemical measurements were performed on the CHI 660E electrochemical station on the

basis of classic three-electrode system. A piece of the synthesized nanomaterials with certain area of 0.5 × 1 cm^2 was utilized as working electrode, while a graphite rod and Ag/AgCl electrode as the counter and reference electrode, respectively. The alkaline solution containing 1 M KOH and 0.33 M urea was applied as electrolyte for all electrochemical measurements. Linear sweep voltammetry (LSV) curves were recorded within the potential window of 1.05 ~ 1.7 V *vs.* RHE at the scan rate of 5 mV/s. Cyclic voltammetry (CV) was performed from 0.865 V to 0.965 V *vs.* RHE at various scan rates to calculate the electrochemically active surface area (ECSA) of the synthesized electrocatalysts. Electrochemical impedance spectroscopy (EIS) profiles were recorded within frequency range of 0.1 Hz ~ 1 MHz at the potential of 0.7 V. All current density was 90% iR-corrected and all potential was referred to RHE. To calculate the ECSA, the specific capacitance factor for metal phosphides here was 40 μF/cm^2.

Density Functional Theory (DFT) Calculations

DFT calculations were conducted by using the Vienna ab initio Simulation Package (VASP)[1]. Perdew-Burke-Ernzerhof (PBE) functional of generalized gradient approximation (GGA) with projector augmented wave (PAW) was applied to describe the electronic structures of materials[2]. The plane-wave-basis kinetic energy cutoff was set to 450 eV. The convergence thresholds of force and energy were set to 0.02 eV $Å^{-1}$ and 1 × 10^{-5} eV, respectively. The k-point sampling of the Brillouin zone was obtained using a 2 × 2 × 1 by the Monkhorst-Pack scheme. The vacuum slab of 18 Å was inserted in the z-direction for surface isolation to eliminate periodic interaction.

Composition investigation

The composition of the material is investigated through ICP, the results of which are listed in Table S1. Considering that the phase of outer compound matches well with that of CoP with partial replacement of Co with Fe elements, the composition is defined as $Co_3O_4/Fe_xCo_{1-x}P$ for calculation. As shown in Table S1, the ratio of Fe/Co is 1:12.7, so we can obtain x=0.292 according to the equation ($\frac{x}{3+1-x}=\frac{1}{12.7}$), which is close to 0.3 in the material. Therefore, the composition of the as-prepared product is identified as $Co_3O_4/Fe_{0.3}Co_{0.7}P$.

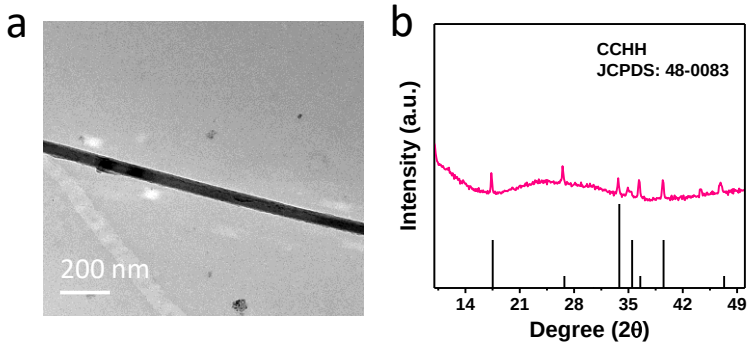

Figure S1. (a) TEM image and (b) XRD pattern of CCHH.

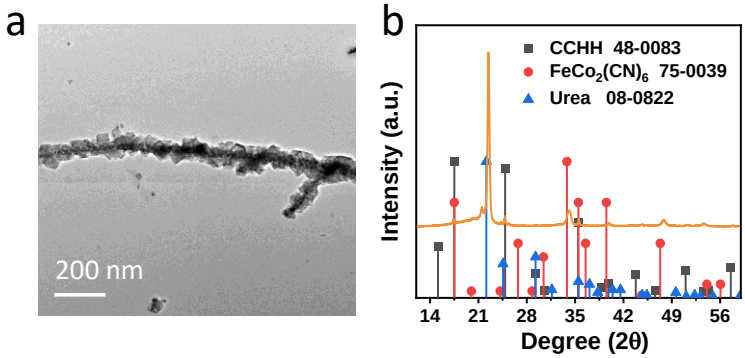

Figure S2. (a) TEM image and (b) XRD profile of CCHH/$FeCo_2(CN)_6$ (the urea is from the reactants).

As shown in Figure S2, there are three kinds of diffraction peaks, where the strong peak of around 22° belongs to urea (JCPDS: 08-0822) from the reactants. The other two groups of peaks are assigned to CCHH (JCPDS: 48-0083) and $FeCo_2(CN)_6$ (JCPDS: 75-0039), respectively, indicating the formation of CCHH/$FeCo_2(CN)_6$ during the synthesis process.

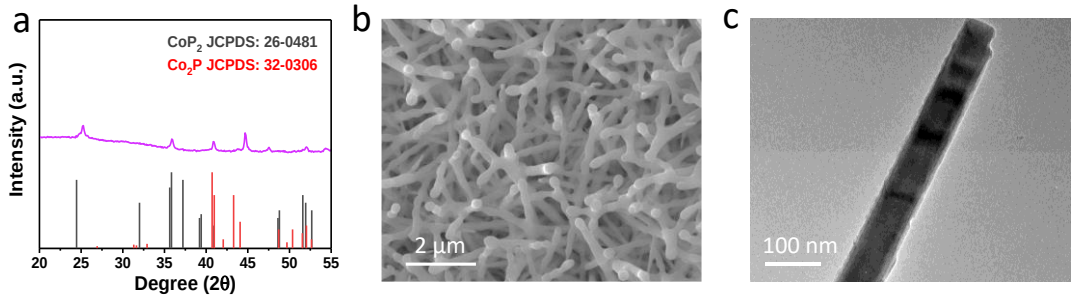

Figure S3. (a) XRD pattern, (b) SEM and (c) TEM image of Co_2P-CoP_2. This sample was obtained when the reaction time of second hydrothermal step was short (3 h), then underwent similar phosphorization procedure. It meant that insufficient etching could not form the heterostructures.

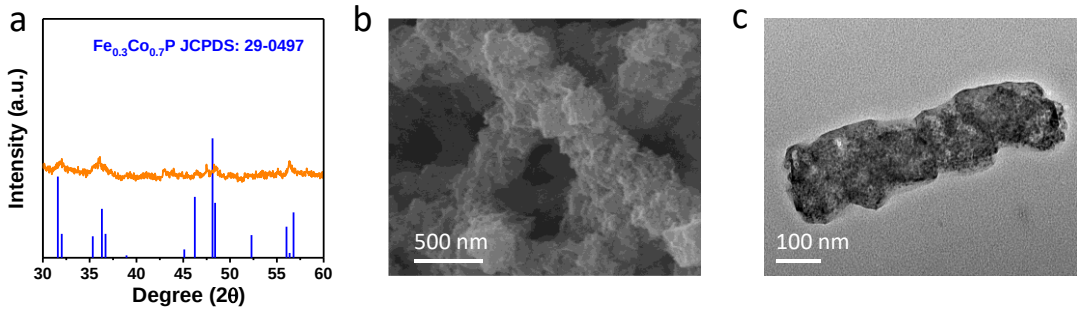

Figure S4. (a) XRD pattern, (b) SEM and (c) TEM image of $Fe_{0.3}Co_{0.7}P$. This sample was obtained when the reaction time of second hydrothermal step was too long (18 h), then underwent similar phosphorization procedure. That explained that the complete etching destroyed the CCHH nanowire, which was harmful for the formation of heterostructures.

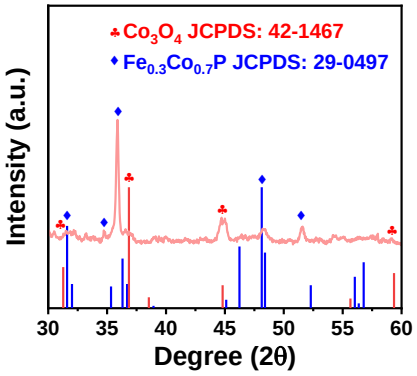

Figure S5. XRD profile of $Co_3O_4/Fe_{0.3}Co_{0.7}P$.

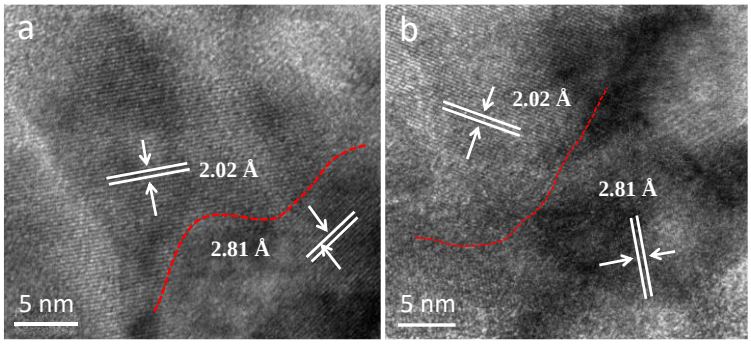

Figure S6. HRTEM images of $Co_3O_4/Fe_{0.3}Co_{0.7}P$, showing the formation of heterointerfaces.

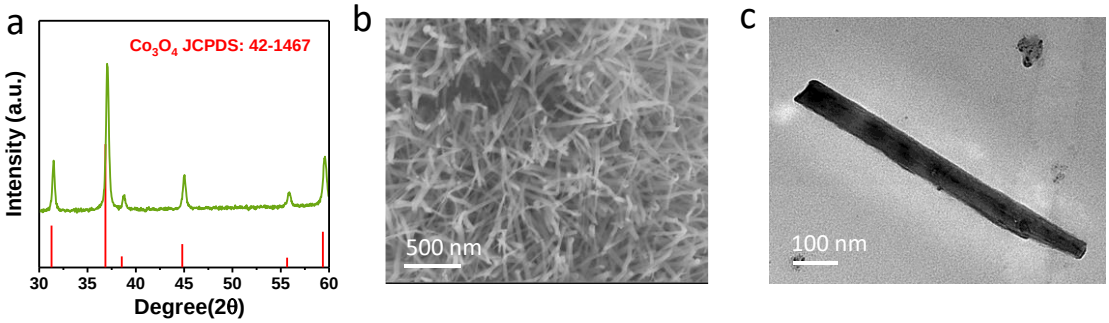

Figure S7. (a) XRD pattern, (b) SEM image and (c) TEM image of Co_3O_4.

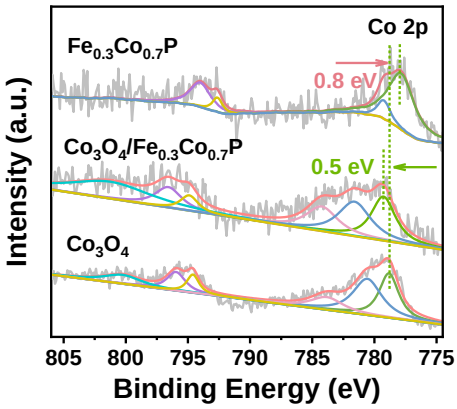

Figure S8. The Co 2p spectra of Co_3O_4, $Co_3O_4/Fe_{0.3}Co_{0.7}P$ and $Fe_{0.3}Co_{0.7}P$.

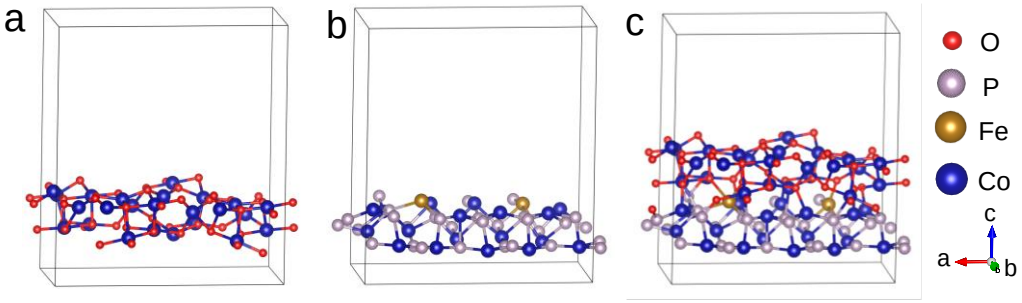

Figure S9. Structure of (a) Co_3O_4 (200), (b) $Fe_{0.3}Co_{0.7}P$ (011) and (c) $Co_3O_4/Fe_{0.3}Co_{0.7}P$ heterostructure, respectively.

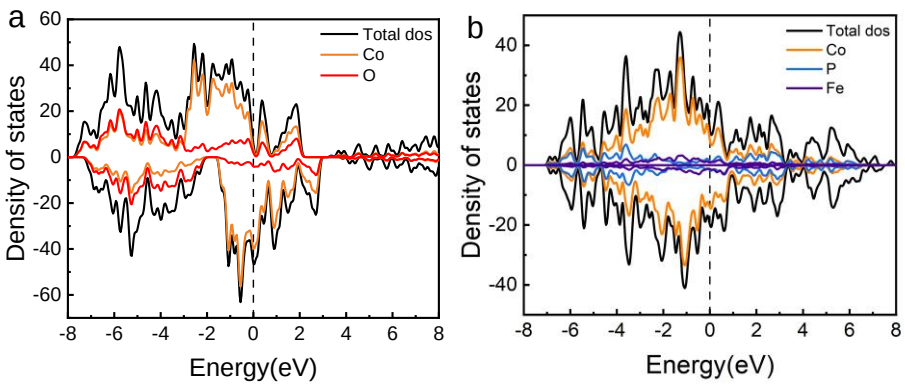

Figure S10. Total DOS of (a) Co_3O_4 and (b) $Fe_{0.3}Co_{0.7}P$, respectively.

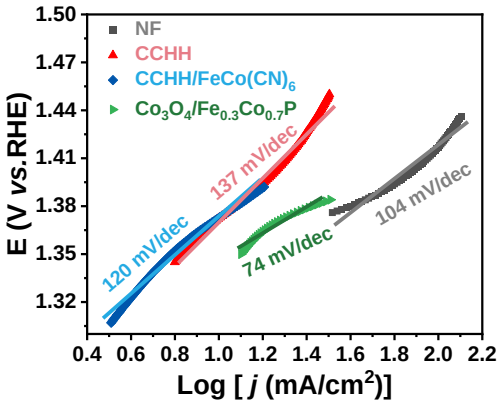

Figure S11. The corresponding Tafel slope of NF, CCHH, CCHH/$FeCo(CN)_6$ and $Co_3O_4/Fe_{0.3}Co_{0.7}P$.

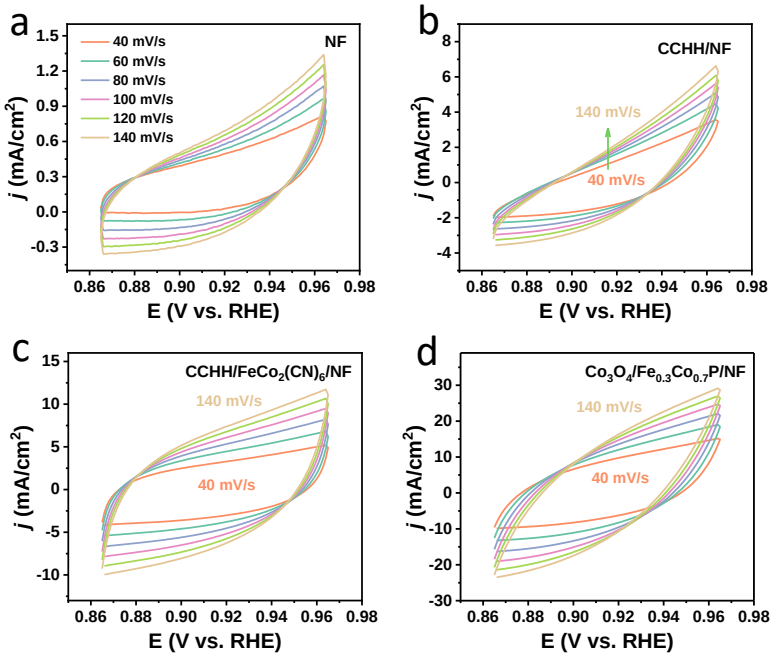

Figure S12. The CV curves of (a) NF; (b) CCHH; (c) CCHH/$FeCo_2(CN)_6$ and (d) $Co_3O_4/Fe_{0.3}Co_{0.7}P$ at various scan rates.

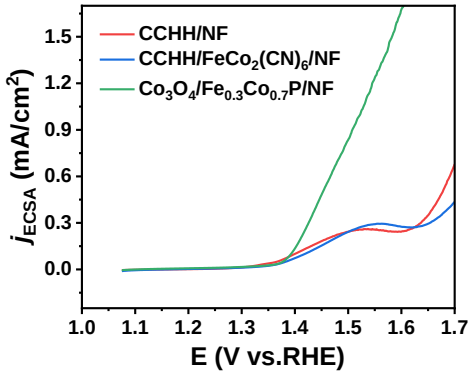

Figure S13. The polarization curves normalized by ECSA of $Co_3O_4/Fe_{0.3}Co_{0.7}P$ and precursors.

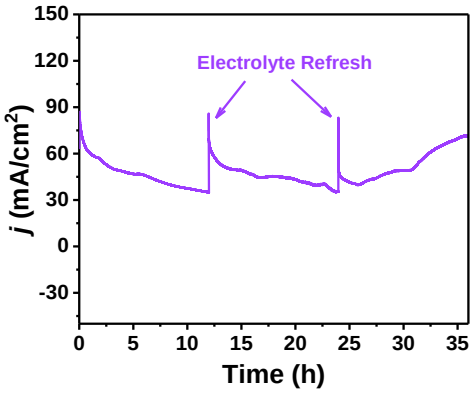

Figure S14. The stability test of $Co_3O_4/Fe_{0.3}Co_{0.7}P$ for UOR.

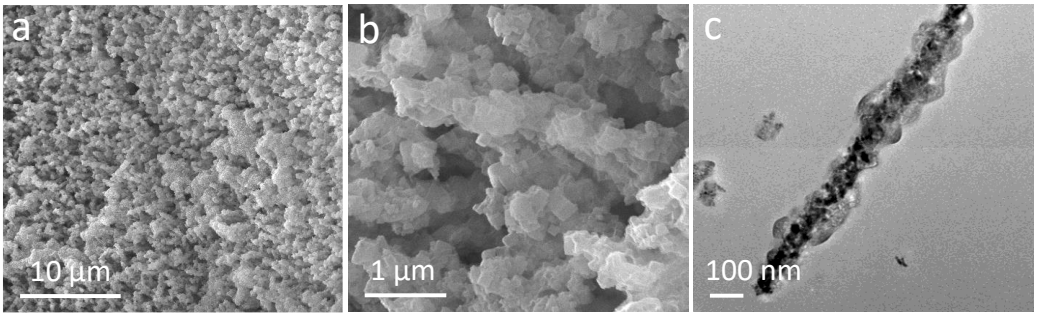

Figure S15. The SEM images (a-b) and TEM image of $Co_3O_4/Fe_{0.3}Co_{0.7}P$ after the stability test.

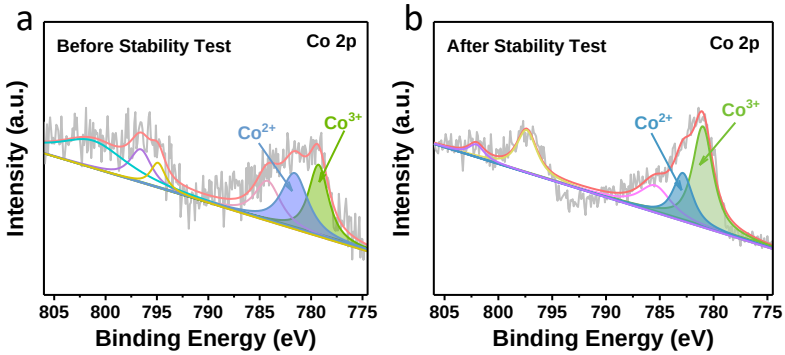

	Co^{3+} ratio	Co^{2+} ratio
Before Stability Test	48.79%	51.21%
After Stability Test	68.56%	31.44%

Figure S16. The XPS spectra of $Co_3O_4/Fe_{0.3}Co_{0.7}P$ before (a) and after (b) the stability test. The corresponding percentage of Co^{3+} and Co^{2+} are shown below.

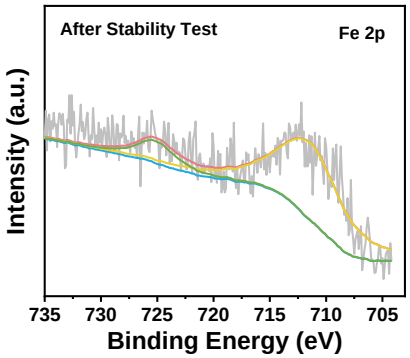

Figure S17. The XPS spectrum of Fe 2p for $Co_3O_4/Fe_{0.3}Co_{0.7}P$ after the stability test.

Table S1. The ICP results of $Co_3O_4/Fe_{0.3}Co_{0.7}P$ and $Fe_{0.3}Co_{0.7}P$.

	Fe (at. %)	Co (at. %)	Fe/Co
$Co_3O_4/Fe_{0.3}Co_{0.7}P$	5.8	73.66	1/12.7
$Fe_{0.3}Co_{0.7}P$	15.3	35.7	3/7

Table S2. The performance comparison of $Co_3O_4/Fe_{0.3}Co_{0.7}P$ and other transition metal-based electrocatalysts recently reported.

Catalysts	η_{100} (V vs. RHE)	Tafel Slope (mV/dec)	Reference
$Co_3O_4/Fe_{0.3}Co_{0.7}P$	1.41	74	*This work*
FeCoNiZn LDH/CC	~1.53	151	J. Colloid Interf. Sci., 2023, 642, 41-52
high-entropy FeCuCoNiZn LDH/CC	~1.47	120	
Cu_3P@CuOx	1.40	29	Appl. Surf. Sci., 2023, 622, DOI: 10.1016/j.apsusc.2023.156925
$CoS_2/MoS_2/Ni_3S_2$	1.43	88.4	Appl. Surf. Sci., 2023, 617, 156621
NiO/MoO_2-1:1	＞1.5	56	Inorg. Chem., 2022, 61, 18318-18324
NiS/MoS_2@CC	1.38	24.2	Chem. Eng. J., 2022, 443, 136321
CoP/NiCoP-350	~1.45	42.8	Mater. Chem. Front., 2022, 6, 1681-1689
NCO/CC 1: 1 (nickel cobalt oxide)	1.43	43	J. Mater. Chem. A, 2021, 9, 8576-8585
V-$FeNi_3N/Ni_3N$	1.42	29.6	ACS Appl. Mater. Interfaces, 2021, 13, 57392-57402
Ni/FeOOH	1.41	26	Chem. Commun., 2020, 56, 14713
nickel-incorporated Co_9S_8	1.43	56	Electrochim. Acta, 2020, 338, 135883

References

1. J. F. G. Kresse, *Comput. Mater. Sci.*, 1996, **6**, 15-50.

2. P. E. Blöchl, *Phys. Rev. B*, 1994, **50**, 17953-17979.